

David B. Wolff<sup>1,2</sup>, D. A. Marks<sup>1,3</sup>, D. Silberstein<sup>1,3</sup>, E. A. Smith<sup>1</sup>, S. W. Bidwell<sup>1</sup><sup>1</sup>NASA Goddard Space Flight Center, <sup>2</sup>Science Systems & Applications, Inc., <sup>3</sup>George Mason University

## 1. INTRODUCTION

The Tropical Rainfall Measuring Mission (TRMM) Ground Validation (GV) Program began in the late 1980's and has provided a wealth of data and resources for validating TRMM satellite estimates, especially at Kwajalein, Republic of the Marshall Islands (KWAJ), and Melbourne, Florida (MELB). The TRMM GV program has provided a full data set (1998-present) of GV products at both sites, which compare well with TRMM estimates (within 10% over open ocean). With the advent of the TRMM Version 6 satellite products, there has been a convergence of both intra-satellite estimates (Precipitation Radar (PR), TRMM Microwave Imager (TMI) and Combined (COM)) algorithms and GV. As the TRMM mission winds down, with the eventual atmospheric re-entry of the satellite, focus has begun in planning for the Global Precipitation Measurement (GPM) GV program. While the main goal of TRMM GV was to provide validation of surface precipitation (rates and accumulations), the main objectives of the GPM GV program are fourfold: (1) to quantitatively assess the error in space-borne precipitation retrievals; (2) to diagnose the sources of space-borne retrieval error; (3) to suggest improvements to the space-borne algorithms to reduce retrieval error; and, (4) to provide quantitative evaluation and improvement of the techniques and algorithms employed in ground validation. This paper describes how TRMM GV data is being used to develop the tools to help meet these GPM GV objectives.

## 2. TRMM GROUND VALIDATION PROGRAM

The TRMM GV program main operational task is to provide rainfall products for four sites: Darwin, Australia (DARW); Houston, Texas (HSTN); Kwajalein, Republic of the Marshall Islands (KWAJ); and, Melbourne, Florida (MELB). Wolff et al. (2005) provide extensive detail on the TRMM GV program, site descriptions, algorithms and data processing. However, subsets of these products, which are referred to in this paper, are described in Table 1.

The TRMM GV group at NASA GSFC routinely generates a number of GV products for use in validating TRMM satellite retrievals. Fig. 1 provides the data flow used to generate these various products. Emphasis of GV data production has been on KWAJ (being essentially an ocean-only site), and MELB (a coastal site with excellent gauge coverage and operational logistics).

*Corresponding author's address:* David B. Wolff, NASA GSFC, Code 912.1, Greenbelt, MD, 20771; e-mail: [wolff@radar.gsfc.nasa.gov](mailto:wolff@radar.gsfc.nasa.gov)

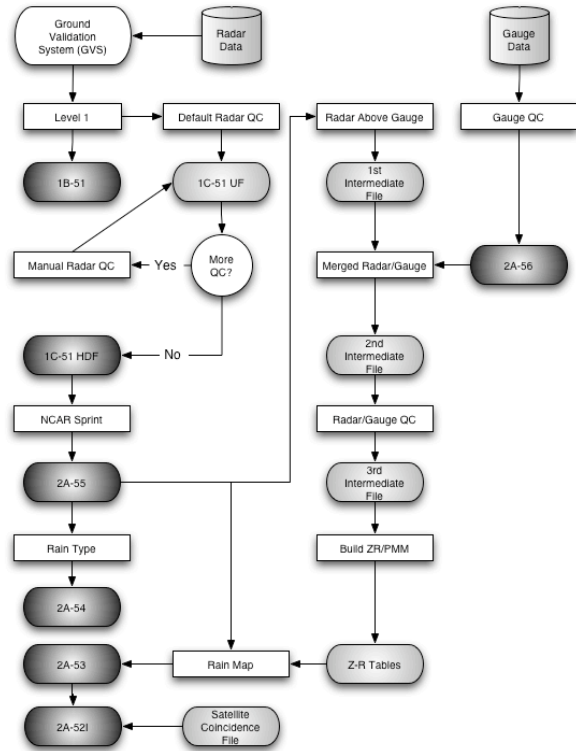


Fig. 1: Data flow diagram for TRMM GV operational data production. Shaded ovals represent official TRMM GV products that are routinely delivered to the TRMM Science Data and Information System (TSDIS).

In general there are three 'levels' of products routinely generated by TRMM GV, which are discussed fully in Wolff et al. (2005). Table 1 provides a description of the subset of the overall TRMM GV product stream that will be discussed or used in the analyses in this study. Obviously, the rain products are integral to the GV effort, so some discussion of the algorithms used to derive rainfall products from ground based radar data is warranted. These products include instantaneous rain maps, convective/stratiform rain type maps, gridded reflectivity, gauge rain intensities and rain accumulation maps.

Product	Fields	Description
2A-53	R	Rain intensity map (2 km x 2 km, extending 150 km from the radar).
2A-56	R	1-minute average gauge rain intensities.

Table 1: Description of GV products discussed in this paper.

## 2.1 TRMM GV SITE DESCRIPTIONS

Figures 2 and 3 provide a geographical map of the gauge and radar networks at KWAJ and MELB, respectively. These maps show the conundrum of TRMM GV, namely, that sites that are principally ocean (such as KWAJ), and provide the best comparisons between the passive microwave (MW) instruments on TRMM, provide only limited real estate for deployment of gauges that can be used for calibration of the GV radar rainfall estimates. On the other hand, sites with substantial gauge coverage lack extensive ocean coverage and indeed contain a significant amount of coastal regions that are quite difficult for passive MW algorithms to handle.

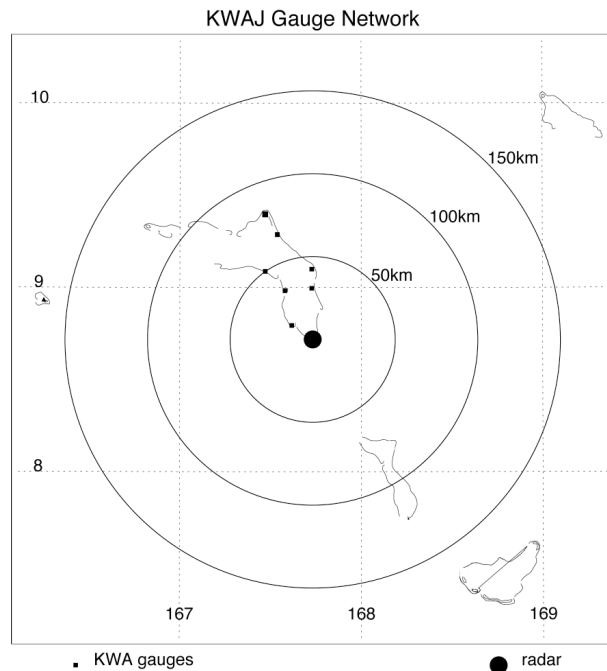


Fig. 2: Gauge and radar network at KWAJ.

In Fig. 2, it is seen that only seven distinct gauge sites are available. In an effort to make sure that the surface rainfall estimates at these limited sites are of the best possible quality, NASA has installed at least two gauges at each site for redundancy. There are several potential problems that may cause a given gauge to fail, many of which are not easy to determine in post processing. There are many possible reasons for these data 'gaps' such as logger dropouts, bad batteries, gauge malfunctions such as a blocked funnel and others.

In Figs. 2 and 3, the primary radar is located at the center of the figure. Range rings depicting distance from the radar are provided at 50 km (KWAJ) and 100 km (MELB) increments extending to 150 km (KWAJ) and 300 km (MELB). We note that the Level II and III GV products, however, are only generated to a range of 150 km from the radar.

Figure 3 provides the gauge and radar network at MELB. There are multiple sources of gauge data in Florida, one of which is operated by NASA at Kennedy Space Center (KSC), while the others are operated by Florida state-sponsored Water Management Districts. The collaboration of these agencies has been extremely valuable for TRMM GV and will certainly play a key role in validation for GPM in the future.

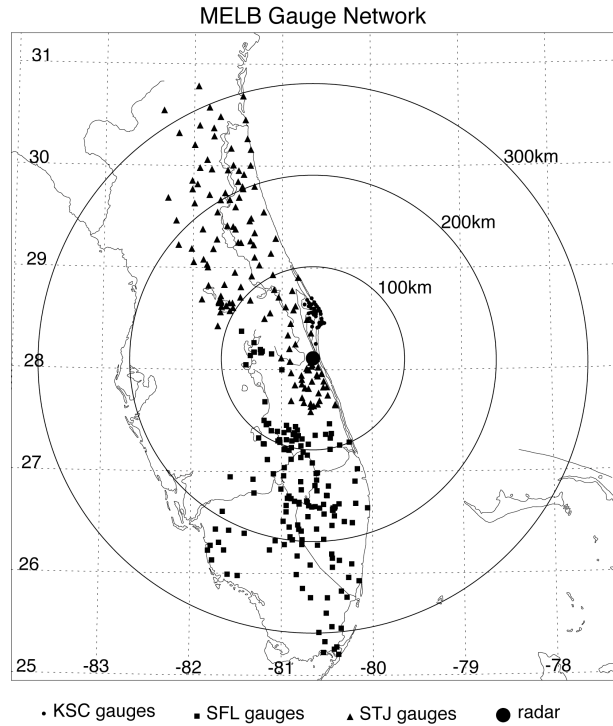


Fig. 3: Gauge and radar network at MELB in Florida.

## 2.2 RAIN ESTIMATION TECHNIQUE

The TRMM GV algorithms have evolved over the last several years in order to improve our rainfall estimates. Early version of the GV algorithms employed a monthly 'bulk adjustment' scheme which used a default reflectivity  $Z$  to rain rate  $R$  relationship ( $Z = AR^b$ ) to convert reflectivity values above the gauges to rain intensities. These rates are then accumulated over an entire month and compared to the gauge accumulations below. The result is a radar-to-gauge (R/G) accumulation ratio that is then applied to the coefficient  $A$  of the default  $Z_e$ - $R$  and this new  $Z_e$ - $R$  is used to re-convert the reflectivity to rain rates. The final result is that the accumulated radar rain estimates matched the gauge measured rain estimates on a monthly scale. It was determined, however, that due to several physical limitations (time synchronization errors, rain advection, evaporation, and many others) that this technique is not robust and did not provide useful values for comparison with TRMM. The Window Probability Matching Method (WPMM, Rosenfeld et al. 1994) is now employed. Rather than requiring the monthly accumulations to match, this technique instead matches the probability distributions of gauge rain rates and radar reflectivity.

Once the distributions are generated, a lookup to table of Z to R is generated for application to the reflectivity data. The current Version 5 GV products use the WPMM for producing its rain estimates. More detail on the implementation of this technique is available in Wolff et al. 2005. For MELB, the number of gauges allows for monthly determination of the WPMM relationships to be generated. At KWAJ, where there are only a limited number of gauges available, we currently use the entire period of 2002 to derive the WPMM relationships which are then applied to all other periods.

### 2.3 ACCURACY OF GV ESTIMATES

How accurate are the current GV rain estimates? The answer to this depends on the site and period, but it is reasonable to say that on a monthly scale, the gauge and radar estimates agree within 10-15%. The magnitude of the errors is largely dependent on radar calibration. At KWAJ, for example, known changes in radar calibration result in large differences in our radar to gauge ratios (R/G). An effort is underway now to develop a technique to determine the relative calibration of the KWAJ radar. This methodology uses the distribution of reflectivity values over known areas of frequent clutter to detect relative changes in the calibration on a day-to-day basis (Wolff et al. 2004). While additional study is necessary to refine this technique, it appears to be a quite robust method to determine these relative changes, many of which have been tied to known engineering issues listed in the radar log book at KWAJ.

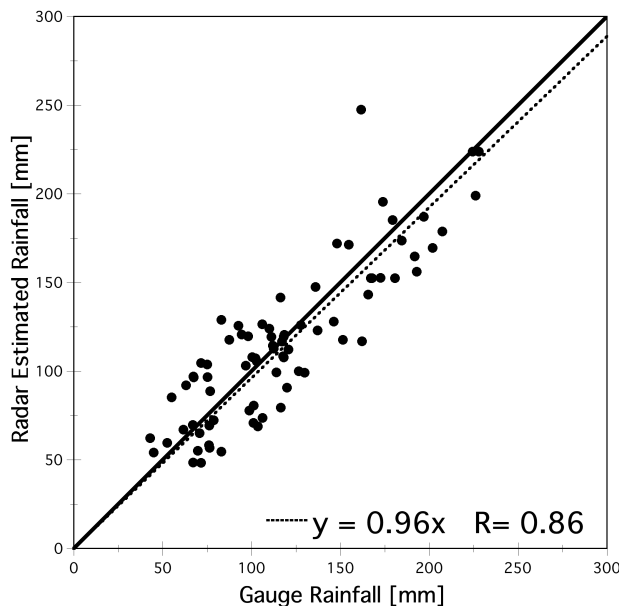


Fig. 4: Scatter-plot of gauge vs. radar accumulations at MELB for August, 1998. Each symbol represents a monthly accumulation (in mm) from the rain gauge (2A-56) and radar estimate above the gauge (3A-54).

Figure 4 provides a scatter-plot of monthly radar and gauge accumulations for MELB during August,

1998. This plot provides an example of dependent validation because the rain gauge data that were used to create the R distribution for the monthly WPMM  $Z_e$ -R are compared here with radar rain rate accumulations. The resulting statistics from dependent validation are basically an algorithm and technique sanity check when considering only the integral R/G from all gauges. In order to provide 'independent' validation of the GV estimates, one must either deploy an independent set of gauges that are not used for rain rate calibration, or compare radar and gauge observations during periods that were not considered in development of the  $Z_e$ -R relationship being used. NASA has deployed a Dense Rain Gauge Network (DRGN) at a site approximately 40 km west of the radar in Melbourne, FL. Figure 5 provides such an independent validation for the same period as Fig. 4 (August 1998). These independent comparisons are well correlated (0.93) and the slope of the regression line (1.07) suggests a 7% overestimate by the radar for this period.

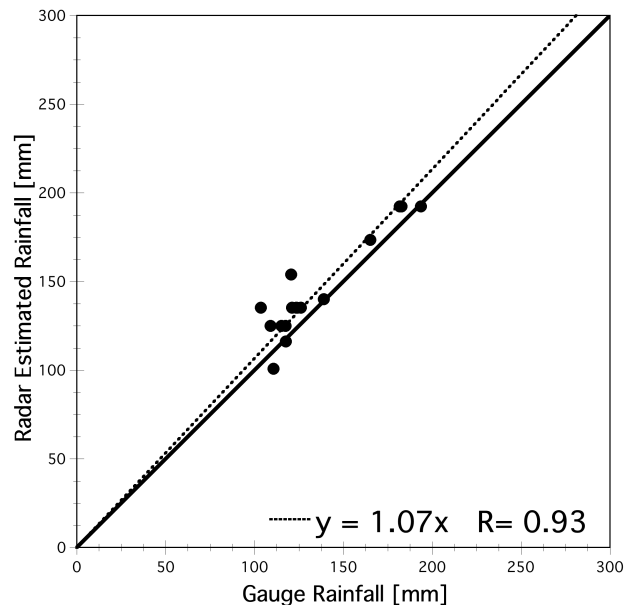


Fig. 5: Same as Fig. 4, except that the gauges plotted were not used in determination of the  $Z_e$ -R algorithm and thus provide independent validation of the radar estimates.

At KWAJ, limited gauge data requires different techniques for providing rain estimates. As noted earlier we use the entire period 2002 to derive the WPMM  $Z_e$ -R relationships. This 2002-based WPMM is then applied to all other periods. Figure 6 provides the dependent validation of monthly rainfall estimates at KWAJ for 2002, because this was the period that was used to develop the WPMM  $Z_e$ -R relationship. The data is well correlated with a coefficient of 0.87 and the slope of the regression line is 0.98, indicating a 2% underestimate by the radar. Figure 7 on the other hand represents independent validation because the period is from 2001.

For this period, the correlation of 0.93 is actually a bit higher, probably due to a recently detected radar calibration change in mid-2002, and the slope of the regression line is 0.96, indicating a slight (4%) underestimate by the radar for the period.

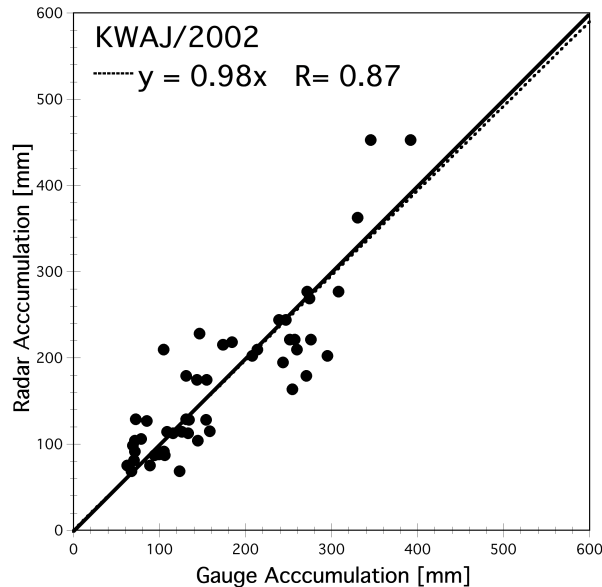


Fig. 6: Scatter plot of monthly radar and gauge accumulations at KWAJ for 2002. Because this period was used in developing the WPMM  $Z_e$ -R relationships, this represents 'dependent' validation.

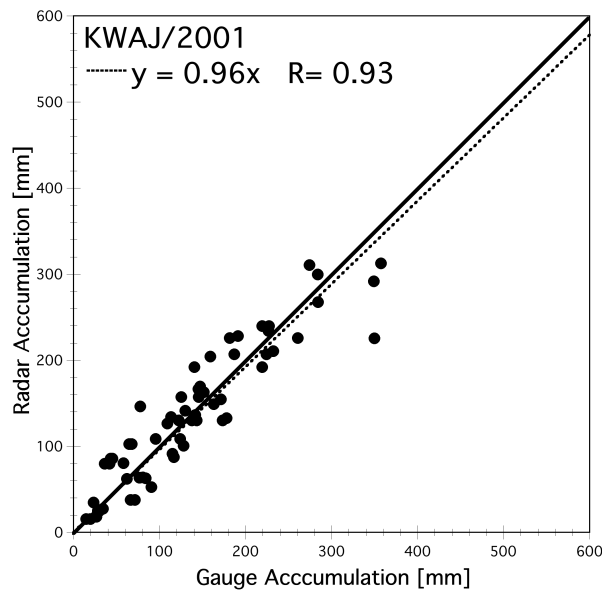


Fig. 7: Same as Fig. 6, except covers entire year of 2001 and thus represents independent validation of the estimates.

### 3. COMPARISONS WITH TRMM RETRIEVALS

As stated earlier, the main goal of the TRMM GV program is to provide rain estimate at various sites

throughout the globe in order to compare with and hopefully help improve TRMM satellite retrievals. This section will show several comparisons of GV rain intensities and satellite retrievals from the TRMM Microwave Imager (TMI), Precipitation Radar (PR) and Combined (COM) algorithms. The TRMM data used for these comparisons was obtained from the 3G68 gridded rainfall product developed by TSDIS. The 3G68 global product provides the average rain rate in  $0.5^\circ \times 0.5^\circ$  pixels for the TRMM Microwave Imager (TMI), Precipitation Radar (PR) and Combined (COM) algorithms. Data from each 3G68 pixel that lay over the respective GV sites was extracted and then compared to TRMM GV estimates obtained by de-resolving the 2 km x 2km 2A53 rain map pixels to the same grid as the 3G68 product. Thus, the comparisons were pixel-matched in both time and space, removing sampling as a source of error in these comparisons.

### 3.1 TRMM LAND, COAST, OCEAN MASKS

Figure 8 provides a map used by TRMM algorithms to determine the surface properties of satellite observations. There are numerous categories available, including, land, coastal-land, coast, water, ocean and ice. In MELB, all types of these surfaces exist except for ice. Determination of these surface types is critical to the proper application of the physics of the satellite retrievals. Over land, scattering is the primary means of determining rain rate for the TMI. Over ocean, emission is the dominant signal. Thus, the physical algorithms for determining the rain rate over these areas changes accordingly. Furthermore, coastal regions provide significant challenges to the physics of retrieval and such estimates are not usually considered robust.

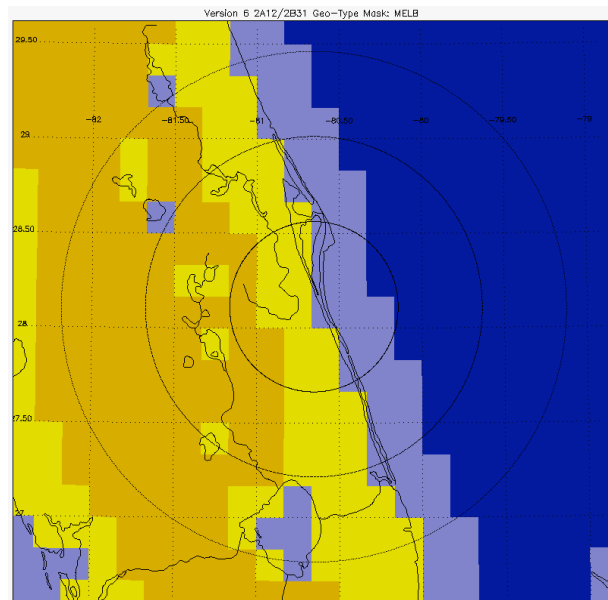


Fig. 8: Geographical type mask used by TRMM. The colors represent the following: dark Blue (ocean); light blue (coast and water), yellow (coastal land); and brown (land).

Figure 9, on the other hand shows the ocean-only characteristic of the KWAJ site and thus highlights the importance of KWAJ to TRMM. From the masks illustrated in Figs. 8 and 9, the GV data was subsampled and characterized according to its surface type. Figure 10 provides the 0.5° x 0.5° mask that was used for this study. Each 0.5° pixel within the GV domain was classified as land (L), coast (C), or ocean (O).

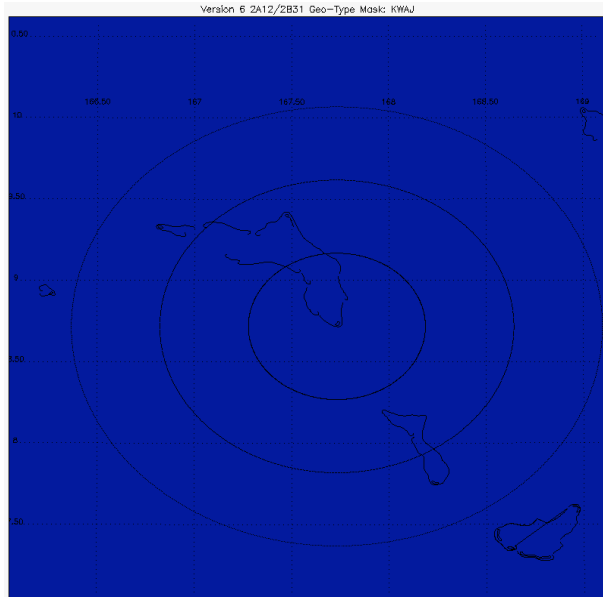


Fig. 9: Same as Fig. 8 except for KWAJ. Blue represents ocean-type surface characteristics.

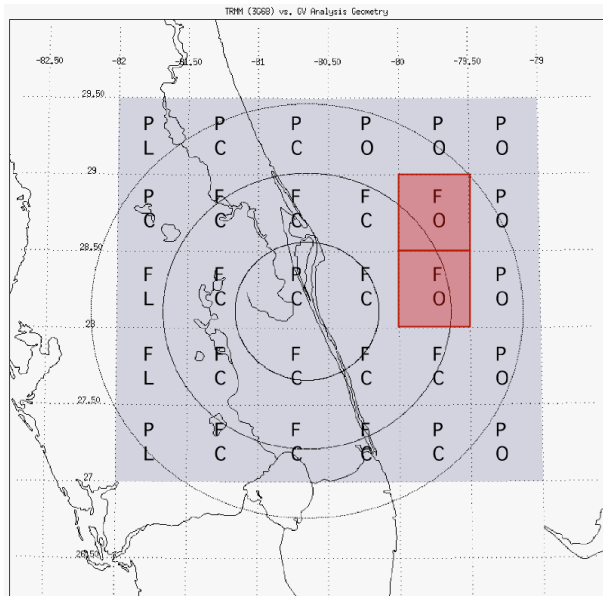


Fig. 10: Mask of GV-constrained surface type for MELB: 'P' is for partial; 'F' is full; 'O' is ocean; 'C' is coast and 'L' is for land. Only 'Full Ocean' (FO) pixels were considered in the current study and are highlighted in red.

Further, if a given pixel was categorized by more than one surface type, an additional classification of 'partial' (P) was made, otherwise it was classified as 'full' (F). Also, if the pixel in question contained any area less than 15 km or more than 150 km from the GV radar, the pixel was also classified as 'partial'. For the present study, only pixels that were classified as "Full Ocean" (FO) were considered and are highlighted in red in Figs. 10-11. It is important to note that KWAJ provides a large number of FO pixels being principally oceanic, but that MELB provides only two FO pixels to compare. Thus differences in the number of available comparisons between each site may lead to some of the differences in the overall biases reported here.

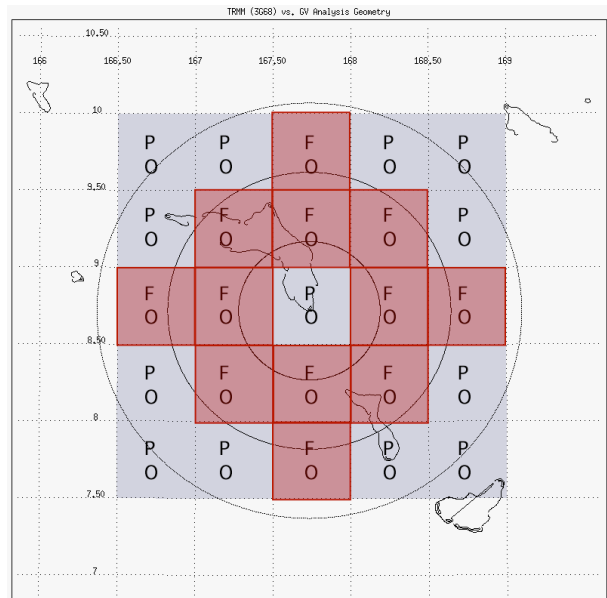


Fig. 11: Same as Fig. 10 except for KWAJ.

### 3.2 OVER OCEAN RAIN COMPARISONS

Now we are ready to present a comparison between GV and TRMM rain intensities. The period that was studied was January 2001 through April 2002 because of the availability of the Version 6a products for TRMM used in testing prior to full reprocessing. As a caveat we note that the final Version 6 is somewhat different from the Version 6a results presented here, but from discussions with the algorithm developers (C. Kummerow, Z. Haddad, R. Meneghini, *personal communication*) we believe that our results will not be significantly changed by the final update. Once the full Version 6 data is available (some time in 2005), we will re-perform our analysis and report the results.

$$Bias = \frac{1}{N} \sum \frac{R - M}{M} \quad 1)$$

The bias, defined in Eq. 1, provides a bulk estimate of the agreement between instantaneous GV and the satellite estimates. In Eq. 1, R is the reference and M is

the measurement or estimate (PR, TMI, COM or GV). We have established three different references, which are shown in Figs. 12 and 13. Basically, we choose as a reference the following: a) GV alone; b) TRMM satellite mean (PR + TMI + COM)/3; and, c) All estimates combined (PR + TMI + COM + GV)/4.

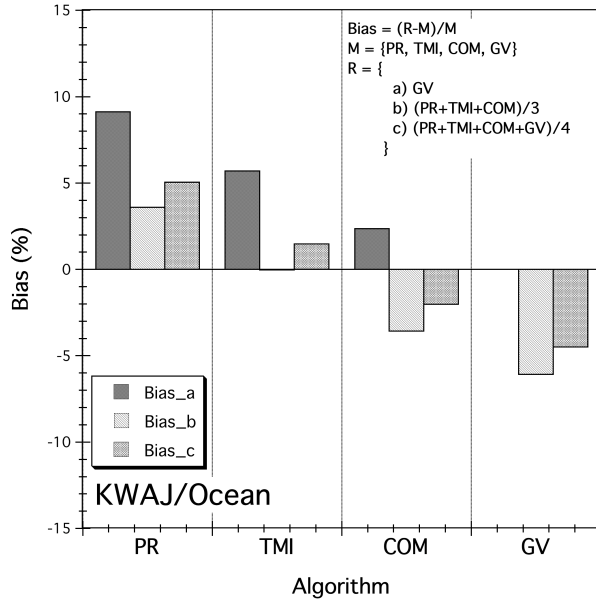


Fig. 12: Overall biases between TRMM satellite estimates and GV in 0.5° boxes over the open ocean at KWAJ. The biases are calculated relative to a reference mean defined by a) GV only; b) Mean of satellite estimates combined; and c) mean of satellite estimates and GV combined.

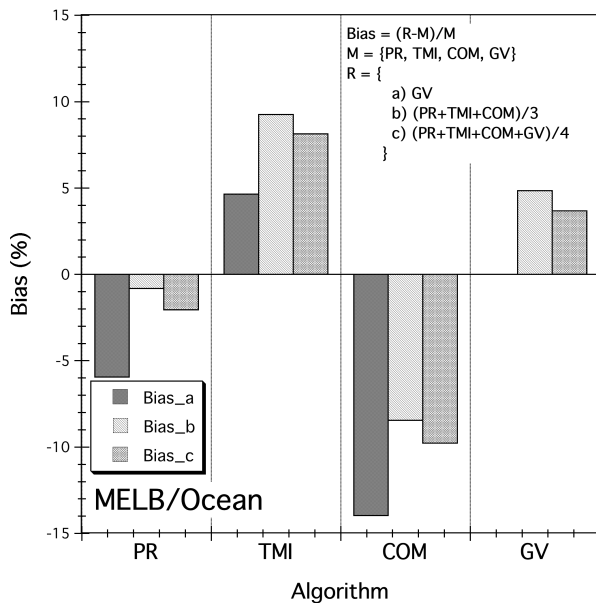


Fig. 13: Same as Fig. 12 except for MELB.

Fig. 12 provides these ‘multi-biases’ for each estimate at KWAJ for period Jan. 2001 – Apr. 2002. The

biases are computed for each estimate, PR, TMI, COM and GV and also for each reference. It is shown that the biases for the PR, relative to the references are highest, but still within +5% to +10%. The TMI fair better with biases in the range of 0% to +7%, and the COM estimates are within -4% to +2%.

Fig. 13 provides the multi-biases over the ocean for MELB. Here, the consistency between the TRMM estimates and GV is not as straightforward, where the PR and COM estimates appear low relative to the references; however, considering the reduced sample size due to limited ‘Full Ocean’ pixels at MELB, the statistics agree well and range from -14% to +9%. It is interesting to note that the COM algorithm is the outlier with large underestimates relative to the references in the range -8% to -14%. This is due to the possible corruption due to coastal effects. The final Version 6 COM algorithm may reduce these differences.

### 3.3 RAIN INTENSITY DISTRIBUTIONS

While comparing bulk means is informative, it does not provide the whole story, as it only makes inferences about a single statistic. A more robust method is to compare the distributions of rain intensities from the various satellite estimates and those from GV. Figure 14 and 15 provide the probability density function (PDF) and cumulative distribution functions (CDF) of rain intensities for both TRMM and GV at KWAJ and MELB, respectively (S. Yang provided the TRMM distributions).

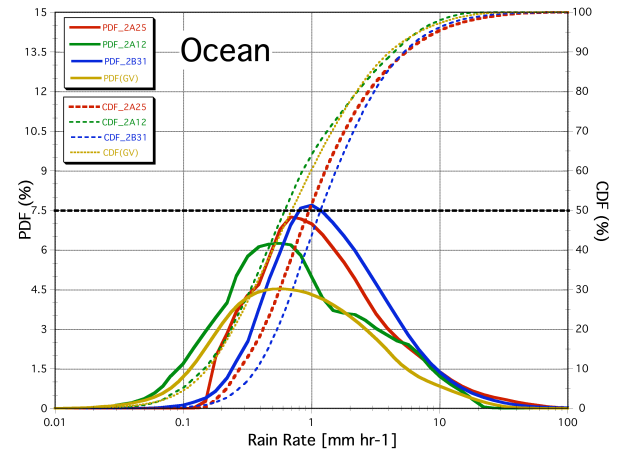


Fig. 14: Comparison of probability density functions (PDF) and cumulative distribution functions (CDF) over open ocean. The TRMM distributions were derived from an entire month (Feb. 1998) of over-ocean satellite data within the TRMM domain. The GV distribution was derived from KWAJ radar rain estimates over the period Jul-Dec, 1999.

The satellite distributions were derived from the 2A-12, 2A-25 and 2B31 TRMM products for the PR, TMI and COM algorithms at the footprint scale. A distinction should be made here that the following distributions are obtained from the respective footprint scale and not from

the 0.5° gridded data. These distributions were derived from ocean-only data observed during February, 2001 over the global tropics. On the other hand, the GV PDF was derived from GV 2A-53 rain intensities (2 km x 2 km pixels) over the period Jul-Dec, 1999. The purpose here is to compare the general characteristics of the distributions, and not to infer specific differences in the given rates or statistics, given that the distributions were derived from different times and locations.

From Fig. 14, all of the PDF appear to be nearly normally distributed, with a few exceptions. Generally, the GV intensities cover a larger dynamic range, which is to be expected given the smaller footprint of the GV pixels. Also, the PR appears to have some problems in the lighter rain rates (0.1-0.5 mm hr<sup>-1</sup>), while the TRMM departs from normality at rates > 1 mm hr<sup>-1</sup>. Overall, however, they compare quite well.

Over land, the differences between the various distributions are starker, as seen in Fig. 15'. Here the TRMM PDF were also derived from footprint observations over February 1998, but only over land. The GV intensities were obtained from land-only GV pixels from the MELB 2A-53 product (2 km x 2 km) during July – December, 1999. The GV distribution is broader and normally distributed. While the PR and COM distributions are quite similar to one another, the TMI differs substantially from them and fails to detect rain intensities less than about 0.6 mm hr<sup>-1</sup>.

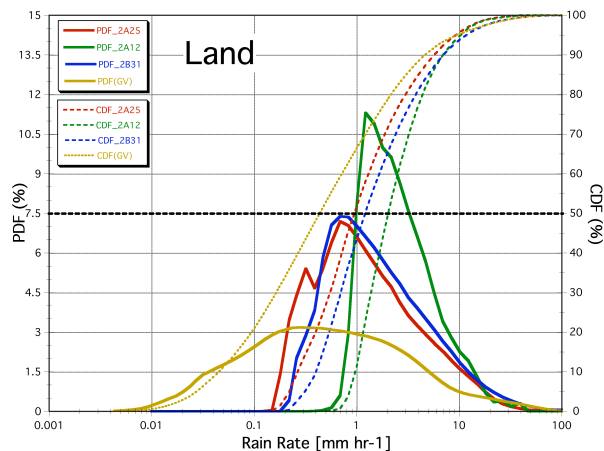


Fig. 15: Same as Fig. 14 except TRMM distributions were derived over land only (Feb. 1998) and the GV distribution was derived from a month of data over land at MELB over the period Jul-Dec, 1999.

The main point to make here is that although the various estimates are converging over ocean, there is still work to be done improving algorithms over land.

#### 4. PLANNING FOR GPM GV

The main goal of TRMM GV was to provide statistical validation of surface precipitation (rates and accumulations); however, as stated previously, the main objectives of the GPM GV program are more robust and

are based on physical validation of the space-based measurements, including 1) determination of the minimum detectable surface precipitation rate; 2) horizontal and vertical spatial mapping of hydrometeors; 3) determination of the spatial pattern of precipitation intensity; and 4) quantitative estimation of surface precipitation rate (Bidwell et al. 2002). In the TRMM era, the available instrumentation to achieve all of these goals were not in place; however, as we have shown here, TRMM GV was effective in providing statistical validation of the surface rain intensities and we will continue to develop these techniques while also looking forward to the GPM era. The most important questions that TRMM and GPM now face are the result of unexplained regional and temporal differences in various TRMM satellite estimates. The TRMM GV group is working with TRMM and GPM algorithm developers to better understand or explain when and why these discrepancies occur. There is some evidence that changes in the drop size distributions and associated assumptions may play a large role in these regional/temporal differences (Berg et al. 2004). GPM mission planning has also considered the fact that additional instrumentation will be required to provide 'physical' rather than statistical validation. Further, historical TRMM and TRMM GV data will be used to develop prototype error-covariance models that may be used in real-time during the GPM era.

#### 5. REFERENCES

- Bidwell, S. W., S. Yuter, W. J Adams, D. F. Everett, G. M. Flemming, and E. A. Smith, *International. Geoscience and Remote Sensing Symposium (IGARSS) 2002*, Toronto, Canada, June 24-28.
- Berg, W. 2004: The Relationship of TRMM Rainfall Biases to the Synoptic Environment. *2<sup>nd</sup> International TRMM Science Conference*, Nara Prefecture, Japan, Sep. 6-10, 2004.
- Rosenfeld, D., D. B. Wolff, and E. Amitai, 1994: The window probability matching method for rainfall measurements with radar. *J. Appl. Meteor.*, 33, 682-693.
- Steiner, M., Houze, Jr., R.A., and Yuter, S.E., 1995: Climatological characterization of three-dimensional storm structure from operational radar and rain gauge data. *J. Appl. Meteor.*, 34, 1978-2007.
- Wolff, D. B., D. A. Marks, E. Amitai, D. S. Silberstein, B. L. Fisher, A. Tokay, J. Wang, and J. L. Pippitt, 2005: Ground Validation for the Tropical Rainfall Measuring Mission (TRMM). *J. Atmos. Ocean. Tech.*, In press.
- Wolff, D. B., E. Amitai, D. A. Marks, D. Silberstein, and J. L. Pippitt, 2004: Status of the TRMM Ground Validation Program at NASA GSFC. *2<sup>nd</sup> International. TRMM Science Conference*, Nara, Japan, Sep. 6-10, 2004.